CB-NOTE 310 10.1.1997

Analysis of channel $\pi^0\pi^0\eta'$ in the 6γ final state of $\bar{p}p$ annihilation at rest

Technical report

Stefan Spanier

Abstract

The final state $\pi^0\pi^0\eta'$ with $\pi^0 \to \gamma\gamma$ and $\eta' \to \gamma\gamma$ is reconstructed using the method of side-bin subtraction. The influence of background from other 6-photon channels is checked by Monte-Carlo simulation and a variation of probabilities of the kinematic fit. A partial wave analysis is applied. The plot can be described with the $\pi\pi$ S-wave in the $\pi^0\pi^0$ subsystem and the $a_2(1320)$ and the $a_0(1450)$ decaying into $\pi^0\eta'$. The decay strength of the $a_0(1450)$ into $\pi^0\eta'$ in comparison to $\pi^0\eta$ is compatible with the expectation of SU(3).

1 Introduction

Due to the small fraction of the decay $\eta' \rightarrow \gamma\gamma$ we expect not many events in the channel $\pi^0\pi^0\eta'$. Despite the fact the the statistics is low , this annihilation channel offers the opportunity to study the $\pi^0\eta'$- decay of $I = 1$ meson resonances ($a_2(1320)$ and $a_0(1450)$). A great advantage is, that phase space switches off the low mass region of the S-wave (the $a_0(980)$ while the $\pi\pi$ S-wave is only seen below the $\bar{K}K$ threshold, where it is rather structureless (σ-region). A disatvantage is the particular distribution of events in the a_2 and a_0 band: since they cross twice within the Dalitz plot. Also the stronger annihilation channels have carefully to be subtracted and their remaining influence has to be well checked.

2 Data reconstruction

The extraction of the signal is based on the all-neutral data sample which already was used to extract the data samples for the coupled channel analysis (see CB-note 274). The run-periods involved are *December'89, June'90, September'90, November'90, May'91, June'91 and August'91*, which all together amounts up to 16.8 Mio events on tape. The following criteria are applied :

1. no charged particle in PWC/JDC
2. 6 PEDs with PED-energy 20 MeV (cluster-energy 20 MeV)
3. events containing PEDs in crystal type 13 rejected
4. minimal energy of a central crystal of a PED greater than 10 MeV
5. apply SMART and merge shower fluctuations.

   Events with one or more unclassified photons are rejected.
6. energy and momentum conservation with the following window :

   $|p_{tot}| < 100$ MeV/c and 1700 MeV$< E_{tot} <$ 2050 MeV

The following table 1 summarizes the selection. See also the following figures displaying the status of the selection parameters.

Events are now subjected a kinematic fit. The errors of the parameters of a photon are scaled depending on the run-period. The fudge factors are listed in table 2. Figures 567 show the pulls of the three photon parameters adjusted by the 4C-fit after a 1% confidence level cut. The superimposed curve shows the expectation for a normal distribution of this quantity. An amount of 1,518,130 events survived the 4C kinematic fit with a confidence level greater than 1%.

Figure 8 summarizes events which survived a 1% probability cut of the several hypotheses. After this exercise a priori 22,381 $\pi^0\pi^0\eta'$ events remain.

	criterium	remaining events
	on tape	16,819,696
1.	no tracks	14,943,119
2.	6 PEDs	3,167,515
3.	crystal 13 cut	2,693,477
4.	energy of central crystal $> 10\,\mathrm{MeV}$	2,359,721
5.	suppression of split-offs	2,221,366
6.	energy/ momentum conservation	1,656,733

Table 1: Preselection of the 6-PED events from the all-neutral triggered data.

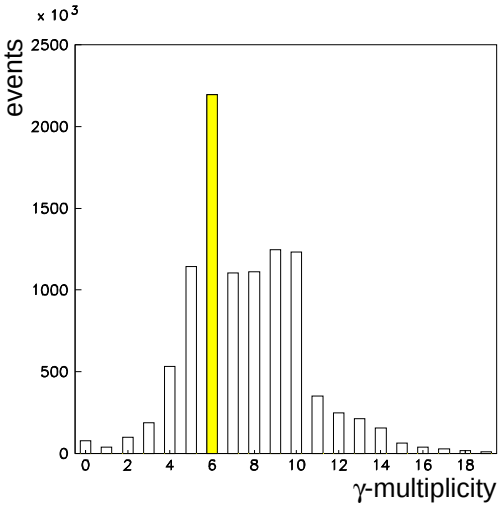

Figure 1:
Distribution of PEDs in the reconstructed all-neutral data-sample.

period	energy	Φ	Θ
12.1989	0.028	1.5	1.5
6.1990	0.028	1.6	1.6
7.1990	0.030	1.6	1.6
9.1990	0.028	1.3	1.3
11.1990	0.026	1.5	1.5
5.1991	0.026	1.6	1.4
6.1991	0.026	1.6	1.4
8.1991	0.028	1.7	1.5

Table 2: Energy errors and fudge factors for several run-periods.

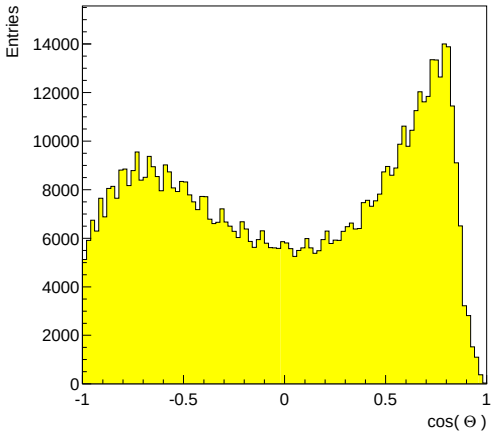

Figure 2:
Shown is the cosine of the opening angle between two PEDs, which show a ratio in the energy of 1:10 and smaller. The missing enrichment of events at $\cos\theta = 1$ signals the suppression of shower fluctuations.

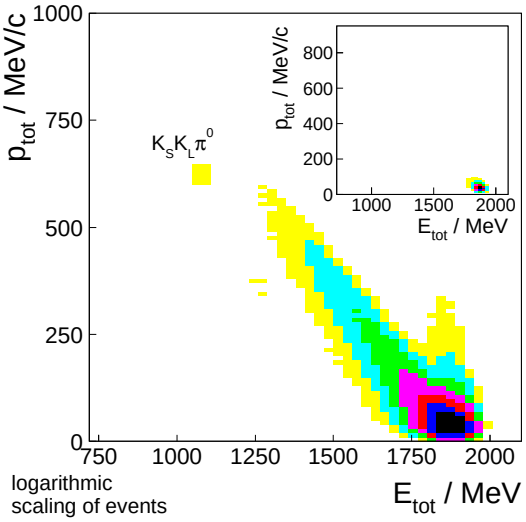

Figure 3:
The total momentum versus total energy of the 6-PED events in a logarithmic z-scale to demonstrate small enhancements (like the channel $K_S K_L \pi^0$). The inlet shows the same plot with a linear scale for the event density. The conservation of momentum and energy clearly visible.

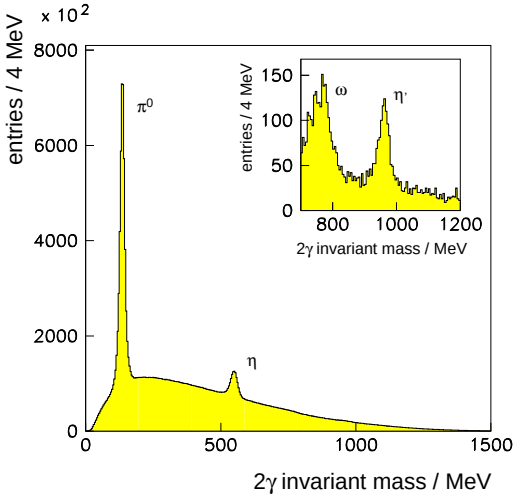

Figure 4:
The 2-PED invariant mass for the 6-PED events (15 combinations). Clearly observable are the π^0 and the η. After subtraction of the π^0 and the η signal the radiative decaying η' and the ω (one γ is misssing) become visible as shown in the inset of the plot. We will concentrate here on the η' peak.

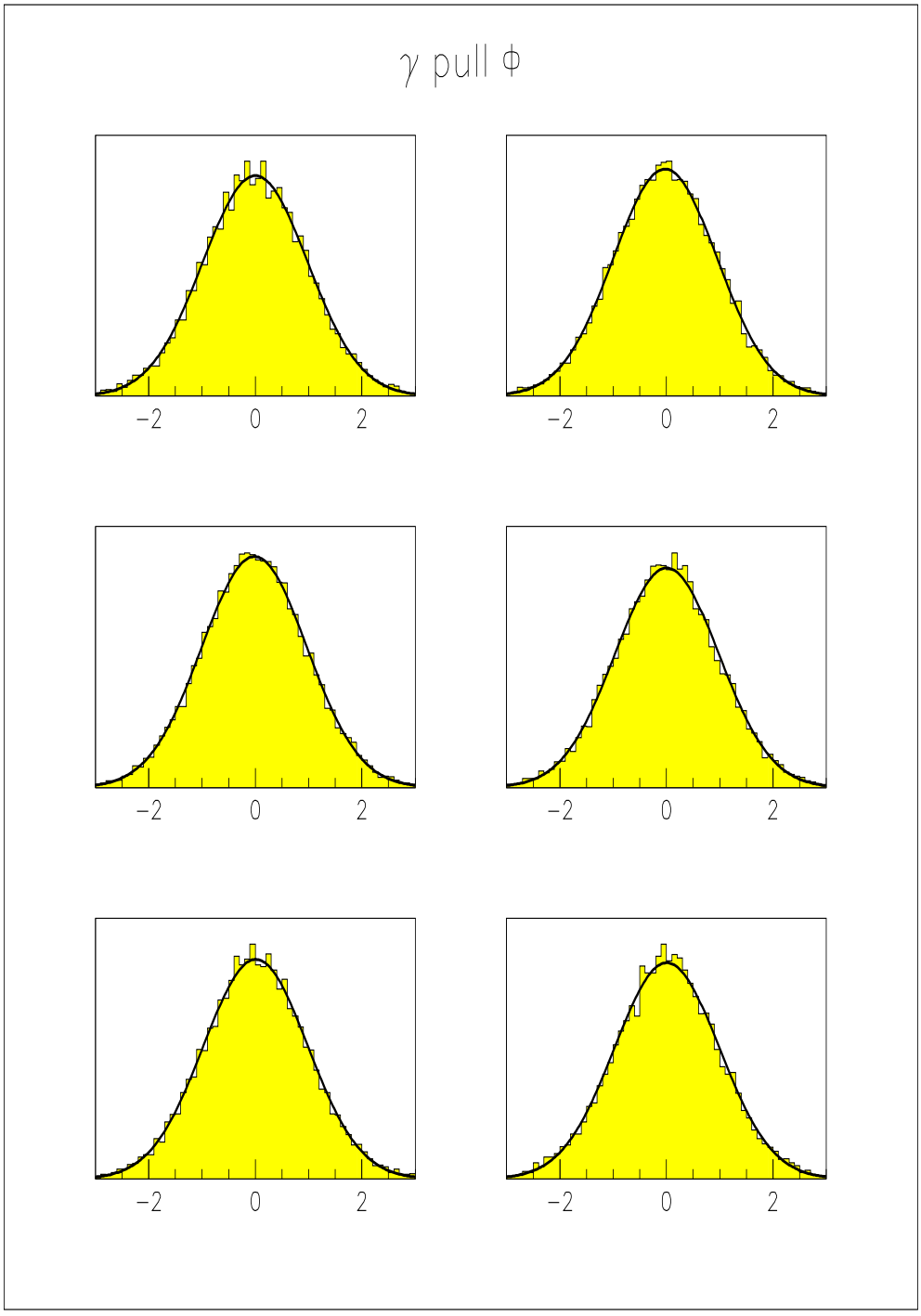

Figure 5: Pulls of the kinematic 4C fit for Φ of the six PEDs.

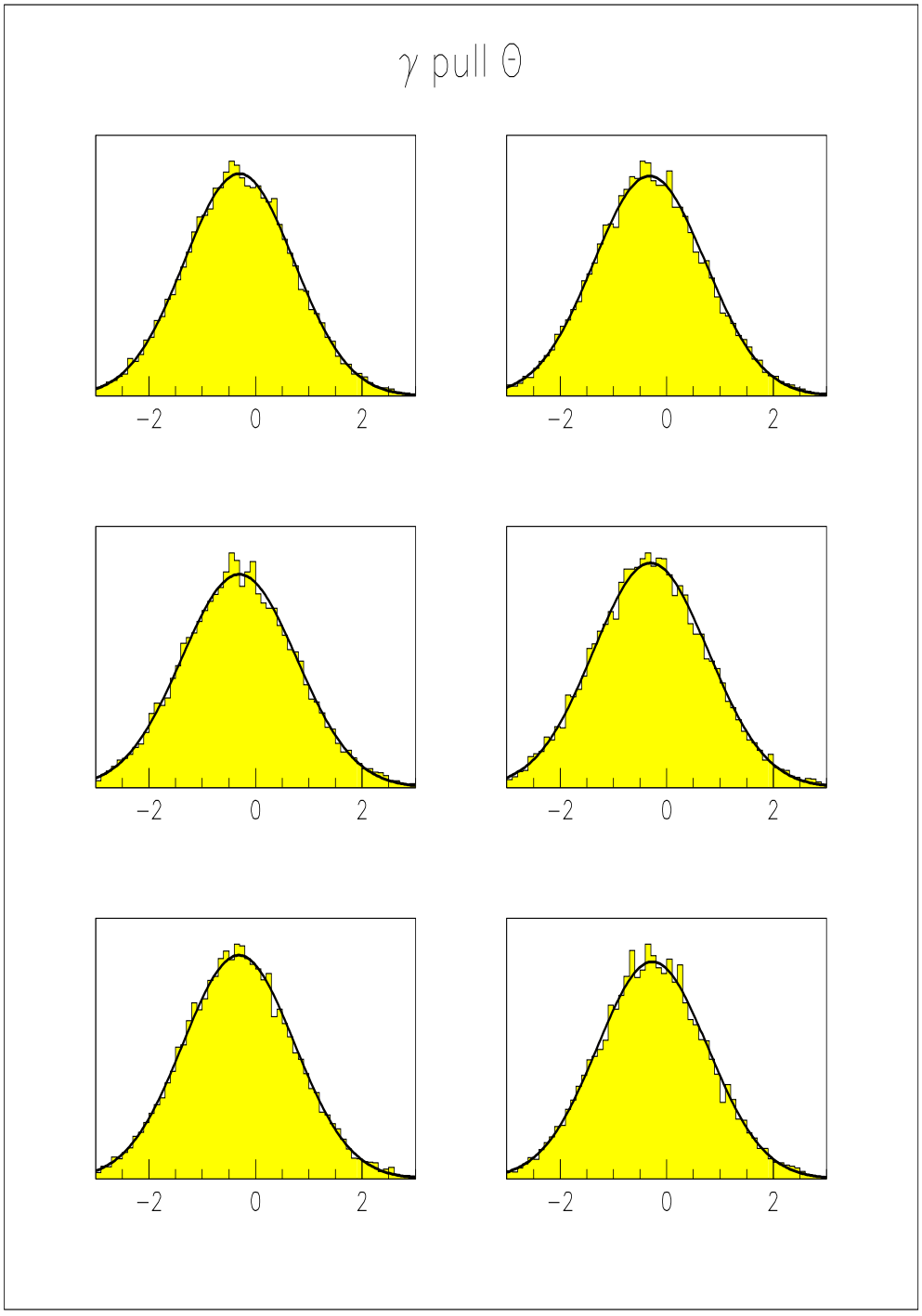

Figure 6: Pulls of the kinematic 4C fit for Θ of the six PEDs.

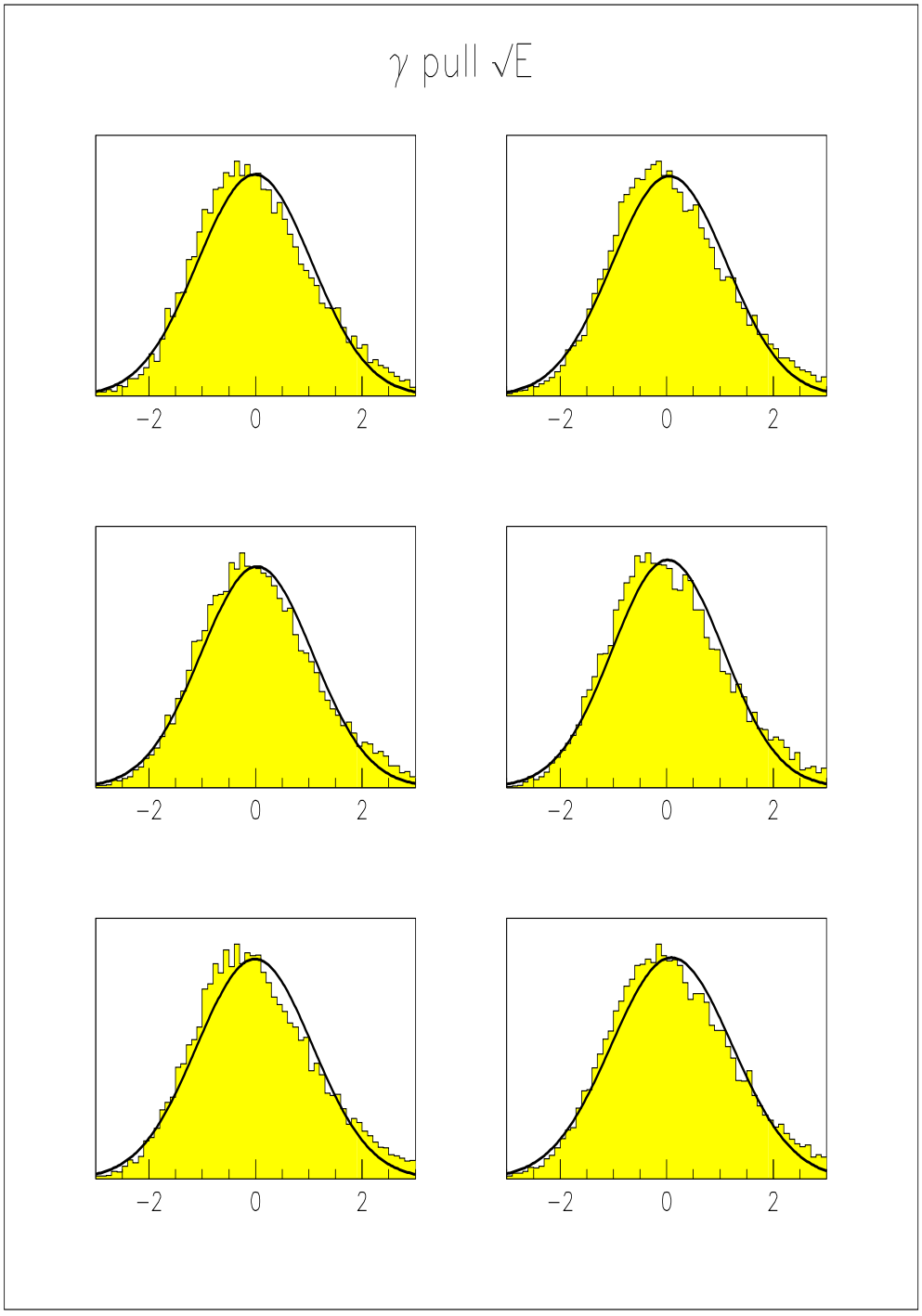

Figure 7: Pulls of the kinematic 4C fit for $\sqrt{E}$ of the six PEDs.

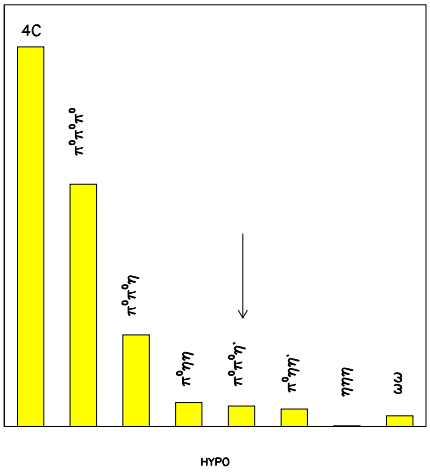

Figure 8:
The distribution of events after application of the kinematic fit to several hypotheses. The interesting channel is marked with an arrow.

3 Selection of $\pi^0\pi^0\eta'$

Further kinematic fit hypotheses are applied and are carefully checked with Monte Carlo simulation, similar to the preparation of the final state $\pi^0\eta\eta'$.

1. After the satisfication of the 4C fit with a confidence level greater than 1%, the strongest channels, namely $3\pi^0$, $\pi^0\pi^0\eta$ and $\pi^0\eta\eta$ are suppressed by the demand, that an event is not allowed to have the highest confidence level for one of them. The confidence level for 7C-fit to $\pi^0\pi^0\eta'$ for and after the cuts is shown in fig. 9.

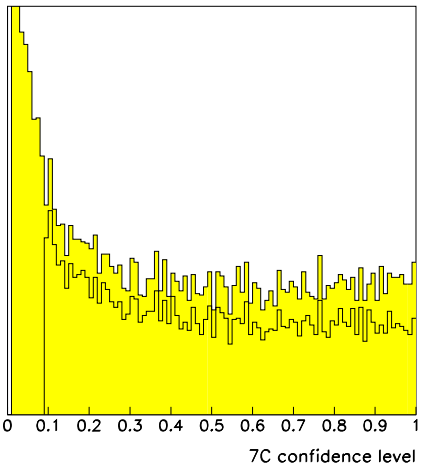

Figure 9:
Confidence level of the 7C-fit to $\pi^0\pi^0\eta'$, before and after the cuts against other channels.

2. The remaining events are subjected to the following 6C fits:
   $\pi^0\pi^0\gamma\gamma$ with confidence level $> 10\%$
   $\pi^0\eta\gamma\gamma$ with c.f. $< 1\%$.
   The remaining $\gamma\gamma$ pair has to come from the signal region (900 MeV$< m(\gamma\gamma) <$ 1020 MeV). The invariant $\gamma\gamma$ mass of the remaining photon pair is shown in fig. 10. We find 6,783 events in the Dalitz plot after this step. Their Dalitz plot is shown in fig. 11.

3. After a repeated 7C - fit for signal and neighbouring regions for background subtraction we arrive at 3,559 events in the Dalitz plot (see next section).

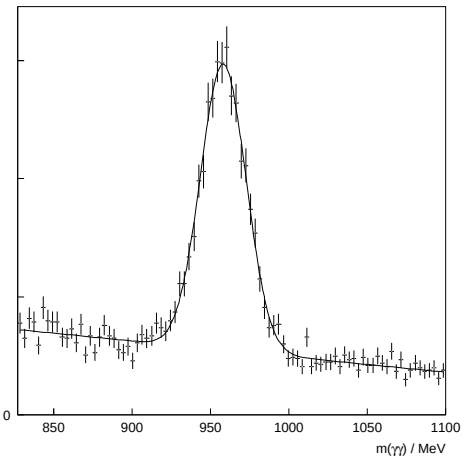

Figure 10:
The η' peak with the fit of a gaussian plus a linear background. One derives a ratio of signal/background of 1.84 ± 0.10.

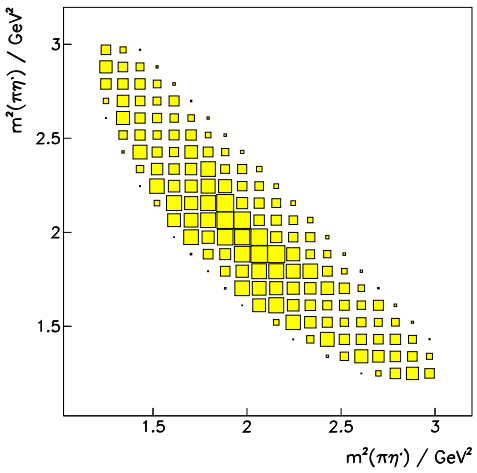

Figure 11:
The distribution of events after application of the kinematic 6C fit.

4 Monte Carlo studies

4.1 Reconstruction efficiency

An amount of 185,800 Monte Carlo events of the type $\pi^0\pi^0\eta'$ with each particle decaying into 2 photons is generated. It is subjected the whole reconstruction chain for the signal region of η'. The confidence level of the 7C-fit to the channel is shown in fig. 12.

Finally, 21,740 events survived. Their distribution over the phase space is shown in fig. 13. From this we calculate a reconstruction efficiency of $\epsilon = (11.7 \pm 0.1_{stat} \pm 1.9_{syst})\%$. The systematic error quoted here accounts for the fluctuation of the event

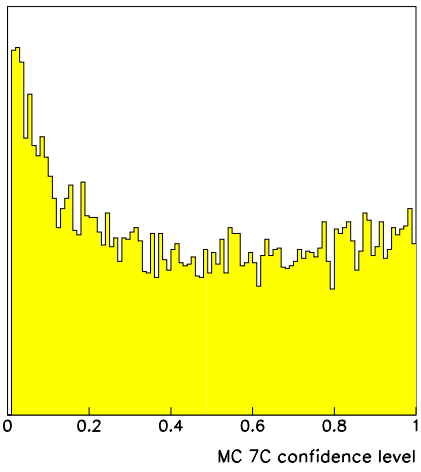

Figure 12:
Confidence level of the 7C-fit to $\pi^0\pi^0\eta'$ Monte Carlos.

density over the phase space. From this plot we extract the relative acceptance correction.

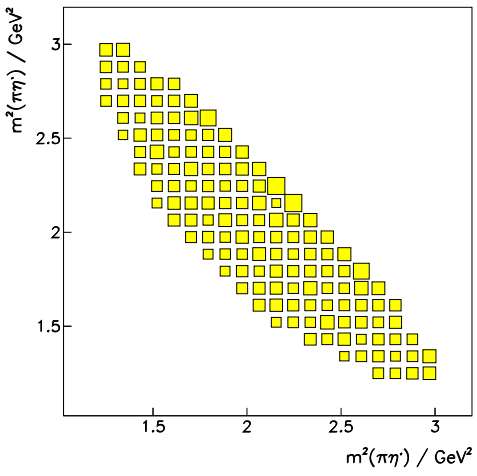

Figure 13:
The acceptance scaling plot for the $\pi^0\pi^0\eta'$ final state from Monte Carlo simulation (area corrected).

4.2 Background

An explicit Monte Carlo study of the possible background channels is performed. The background in the Dalitz plot caused by the competitive channels $3\pi^0$, $\pi^0\pi^0\eta$, $\pi^0\eta\eta$, $\pi^0\eta\eta'$, $\pi^0\pi^0\omega$, $\pi^0\eta\omega$ and $\omega\omega$ sums up to $(12 \pm 1)\%$ after all cuts and is dominated by the channel $\pi^0\pi^0\omega$ (9.8%). The evidence for remaining ω channels after the 6-C fit

can be seen in fig. 14. The resulting distribution of the $\pi^0\pi^0\omega$ events in the $\pi^0\pi^0\eta'$ Dalitz plot is shown in fig. 15.

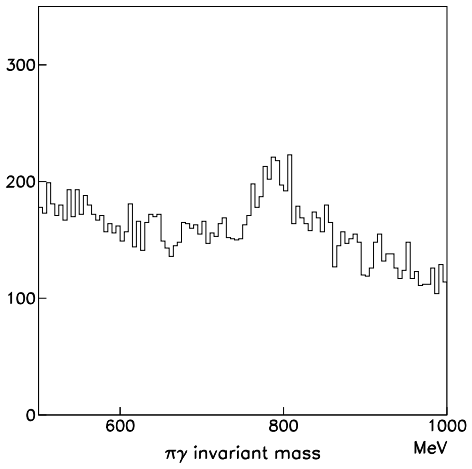

Figure 14:
The $\pi^0\gamma$ invariant mass after application of 6C kinematic fit.

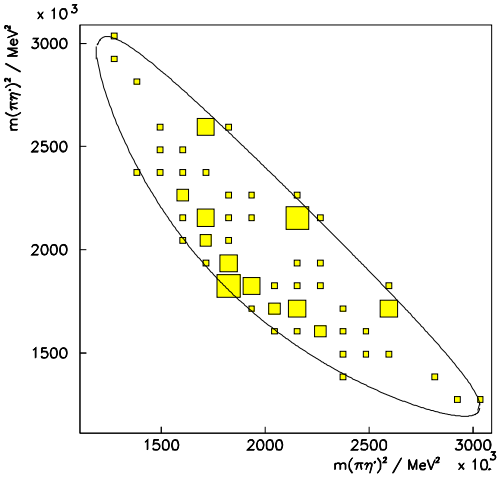

Figure 15:
Simulation of the $\pi^0\pi^0\omega$ background as distributed in the signal Dalitz plot.

As shown by Esther Ferrer [1] by variation of the confidence level anticuts against $\pi^0\pi^0\pi^0$ and $\pi^0\pi^0\eta$, these channels enter the $\pi^0\pi^0\eta'$ Dalitz plot from the outer regions. Setting a rather loose cut against these channels their position in the signal Dalitz plot can be visualized (see fig. 16). A glance to the final Dalitz plot in the next section shows the good suppression of both channels. The $3\pi^0$ conttributes finally about 1% to the $\pi^0\pi^0\eta'$ channel according to Monte Carlo.

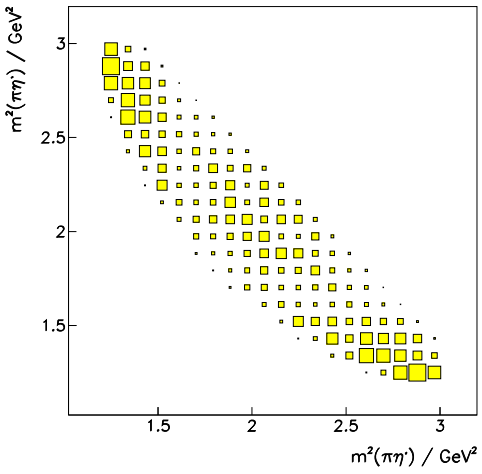

Figure 16:
Demonstration of the $\pi^0\pi^0\pi^0$ and $\pi^0\pi^0\eta$ background if no cuts are applied against them.

The backkground is subtracted using the method of side-bin subtraction. The classification of events from the adjoining regions og the η' signal is based on the 7C-fit. Therefore the mass of the η' is set to the values $m = 877$ MeV and $m = 1037$ MeV, respectively. Both Dalitz plots have to be kinematically corrected. The constraint for the correction is, that angular distributions in the Dalitz plot are not allowed to change. This is achieved by the conservation of particle momenta : The momenta of the photons originating from the η' are multiplied by a factor α to be determined. The invariant mass has to yield the η' mass. Also the momenta of the two pions are scaled independently. The four additional constraints are momentum and energy conservation for the $\pi^0\pi^0\eta'$ events (all together 5 equations). Both side bin Dalitz plots fit now into the signal phase space. Events per Dalitz plot cell from left and right side are averaged. The Dalitz plot constructed from the side bins is shown in fig. 17. The ratio of events in the side bins to the events in the signal is 1.85 in agreement with the determination from the $\gamma\gamma$ spectrum.

Finally we have $(3,559 \pm 60)$ events in the Dalitz plot. The final Dalitz plot is shown in fig 18.

4.3 Branching ratio

Now lets calculate the branching ratio. A possible way to calculate the number of $\bar{p}p$ annihilations uses the channel $\omega\omega$. Even if there may be problems with the reproduction of the ω lets start with it. The number we are looking for is given as :

$$N_{\bar{p}p} = \frac{N_{\omega\omega}}{\epsilon_{\omega\omega}} \frac{1}{B(\bar{p}p \to \omega\omega) B(\omega \to \pi^0\gamma)^2 B(\pi^0 \to \gamma\gamma)^2} \tag{1}$$

For the number of $\omega\omega$ events we rely on the previous selection [2], $N_{\omega\omega} = 5859 \pm 65$

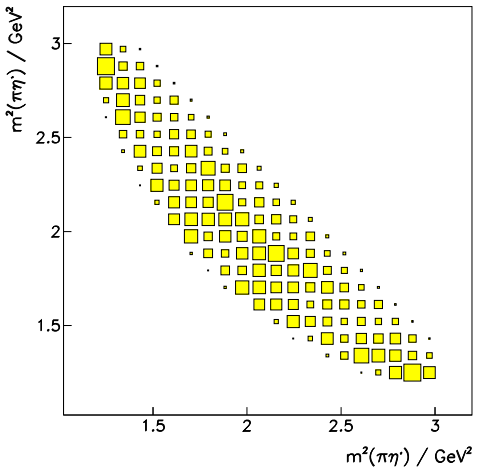

Figure 17:
The total sidebin Dalitz plot to be subtracted from the signal plot.

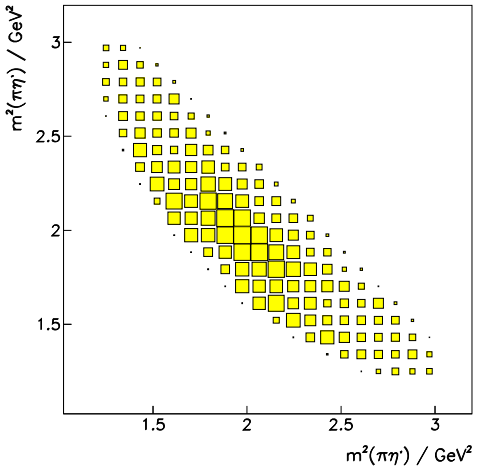

Figure 18:
The $\pi^0\pi^0\eta'$ Dalitz plot (3,559 events, two times plotted), acceptance corrected and background subtracted.

and the branching ratio is $B(\bar{p}p \to \omega\omega) = (3.32 \pm 0.34)\%$ [3]. The reconstruction efficiency in [2] is $\epsilon_{\omega\omega} = 0.0626 \pm 0.0006$. With $F(\pi^0 \to \gamma\gamma) = 0.9880 \pm 0.0003$, $F(\omega \to \pi^0\gamma) = 0.085 \pm 0.005$ we arrive at $N_{\bar{p}p} = (399.7\pm) \cdot 10^6$ annihilations. From these number we can calculate the branching ratio for our channel to be

$$B(\bar{p}p \to \pi^0\pi^0\eta') = (3.7 \pm 0.8) \cdot 10^{-3} \qquad (2)$$

On the other hand the 3,559 events come from 14,534,000 events with no charged track. Assuming that the latter number represents 4% of all annihilations, we get a ratio, which is a factor of 1.1 higher.

5 Partial wave analysis

The at rest annihilation channel $\pi^0\pi^0\eta'$ is expected to contain the intermediate states $a_2(1320)$ and $a_0(1450)$ in the $\pi^0\eta'$ subsystem and the low energy part (σ-region) of the $\pi^0\pi^0$ S-wave. The first two resonances are formulated as 1×1 K-matrices with one or more open channels, corresponding to the known Breit-Wigner formula with energy dependent width [4]. The $\pi^0\pi^0$ S-wave is adopted from the coupled channel analysis [5], but all values are fixed. Different combinations of these contributions will be tested now.

5.1 Procedure

The data sample contains not many events, which means for a chisquare fit of the Dalitz plot the regions of no dynamical activity are difficult to handle. Therefore, a maximum likelihood fit is used in the binned version. The quantity to be minimized is formulated as an equivalent chisquare according to [6]. (just for comparison I will mention the values of the (least squares) chisquares applied usually, the Neyman (error calculated from data) and Pearson (error calculated from theory) quantities.) Assuming a Poisson statistics for the event-number per Dalitz plot bin one arrives at the Poisson likelihood chisquare [6] :

$$\chi^2_L = 2\sum_i y_i - n_i + n_i \ln(n_i/y_i), \tag{3}$$

where n_i the number of events in the i-th bin and y_i the number of events predicted by the model in the i-th bin. The trick for the formulation in such a way is the application of the likelihood ratio test (see PDG).

Each partial wave is normalized individually by integration over the phase space. In particular if one is not able to provide a good description of the final state the individual waves will not sum up to 100% intensity.

As a standard procedure only production strengths were adjusted. Masses and widths were taken from earlier determinations in three pseudoscalar final states. I will also show a mass scan for the $a_0(1450)$.

5.2 Hypotheses

The succesful assumption of a dominance of annihilation from initial S-states of the $\bar{p}p$ system is applied. Only the $^1S_0$ initial state is allowed.

First, the $\pi^0\eta'$ resonances appear two times in an unfortunate way: they strongly overlap. This means a complication in the determination of a $a_0(1450)$ significance and its intensity. The generics of the two $\pi^0\eta'$ resonances are shown in fig. 19. The $a_2(1320)$ parameters are: $m = 1318.4$ MeV and $\Gamma = 107$ MeV.

It turned out, that the formulation of the $\pi\pi$ S-wave is less critical. A good fit is already obtained ($\chi^2_{N_{dof}} \approx 1.3$) by just introducing phase space ($A_{\pi\pi} = 1.0$). The

No	fit	χ^2	$\pi\pi$ S-wave	$\pi^0\eta'$ S-wave	$\pi^0\eta'$ P-wave	$\pi^0\eta'$ D-wave
1	(best)	130	92.8%	4.8%	-	2.0%
2	(no a_0)	310	96.9%	-	-	1.1%
3	(no a_2)	277	73.8%	4.6%	-	-
4	(+ ρ)	126	96.7%	0.7%	0.7%	1.9%
5	(+ ρ - a_0)	132	94.7%	-	1.4%	2.2%
6	(+ ρ + a_0)	113	91.5%	0.6%	0.6%	1.9%

Table 3: Different hypotheses fitted. The individual contributions are *not* renormalized to 100%.

formulation of the S-wave in therms of the 2×2 K-matrix from the analysis of the $3\pi^0$ channel [7] and the 3×3 K-matrix from the coupled channel analysis [5] are more adequate, but practically cannot be distinguished from a formulation with just a broad Breit-Wigner resonance (σ with a width of about 500 MeV).

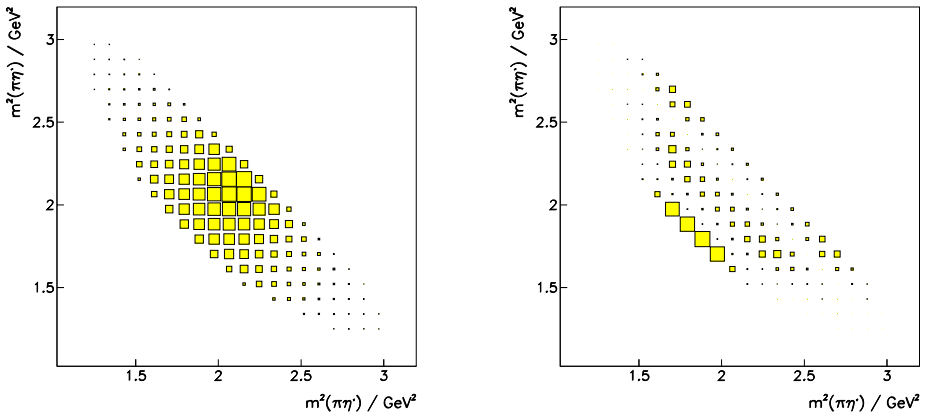

Figure 19: The amplitude squared of the $a_0(1450)$ and the $a_2(1320)$ resonance.

The plots for the best fit are the following : The data Dalitz plot provides 138 filled cells for the fit. In fig. 20 left side the chisquare distribution is displayed. It contains two (twofold) cells with a somewhat higher deviation, which are close to the phase space boundary and in a region of strong acceptance variation. However, they do not show any link to tested dynamical structures. The theoretical Dalitzplot is shown in fig. 20 right , the projection into the $\pi^0\eta'$fig. 20 lower left and the $\pi^0\pi^0$ subsystem fig. 20 lower right (the error bars in the Dalitz plot projections are meaningless, but here are given as approximate variation interval). The mass value

preferred for the hypothesis tests was $a_0(1450)$ is $m = 1490$ MeV and for the width $\Gamma = 280$ MeV. Table 3 gives a compilation of the different hypotheses tested.

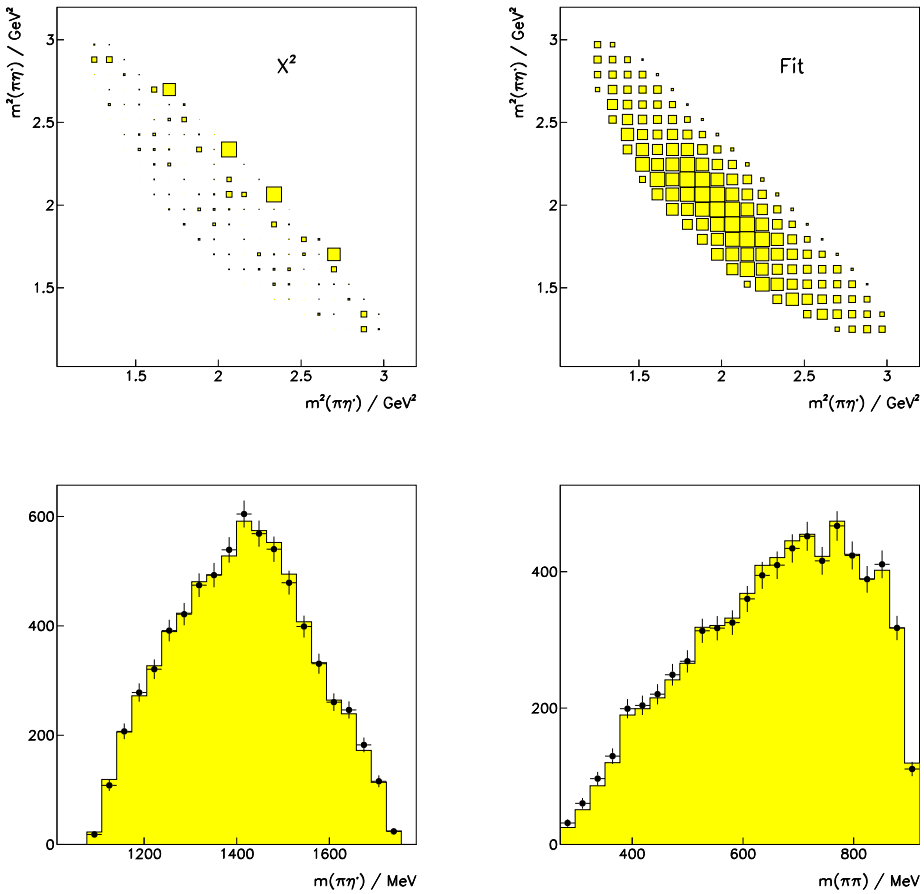

Figure 20: Chisquare Dalitz plot (upper left), the fitted Dalitz plot (upper right) corresponding to the best hypothesis No. 1, and the two projections into the $\pi^0\eta'$ (lower left) and the $\pi^0\pi^0$ (lower right) subsystem. The error bars in the projections only approximate the variation interval for the fit and are calculated from the corrected data Dalitz plot.

Omitting the $a_0(1450)$ results in a increased chisquare. The corresponding plots are shown in fig. 21.

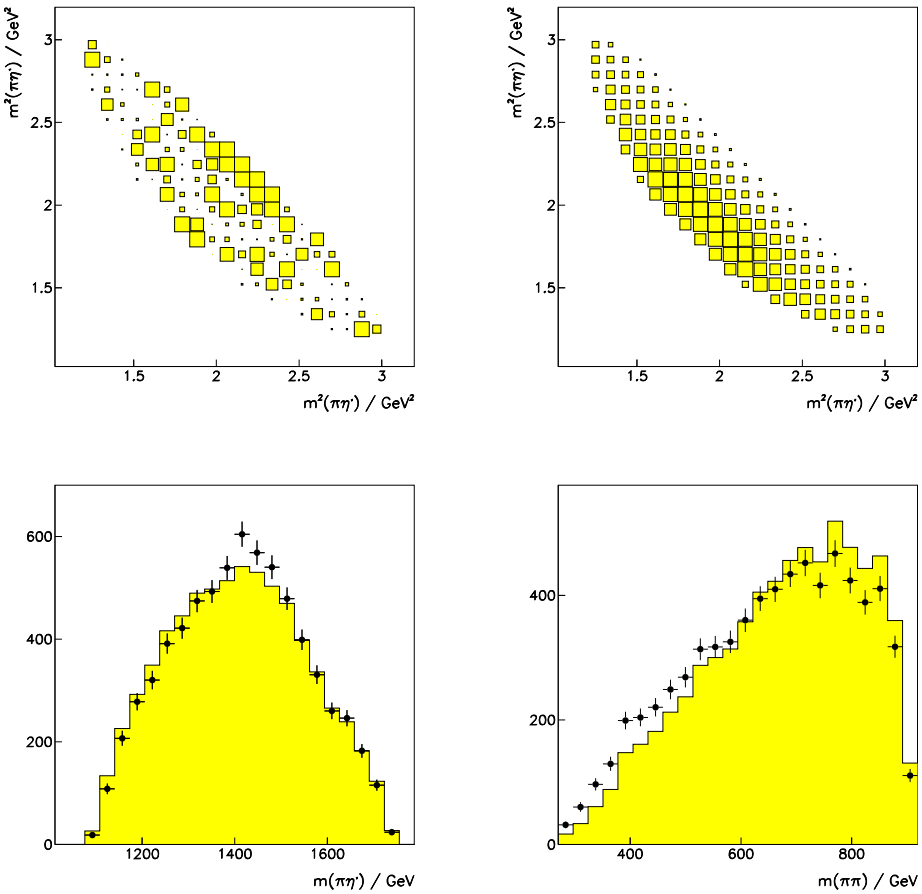

Figure 21: The theoretical Dalitz plot in the best adjustement to the data if $a_0(1450)$ is omitted (hypothesis 2). The two projections are shown in the lower part.

The presence of $a_2(1320)$ is significant, but less than for $a_0(1450)$. The introduction of the P-wave ($m = 1405$ MeV and $\Gamma = 300$ MeV) in addition to the best hypothesis does not change much in the chisquare, but a minimum is reached with a lower $\pi^0\eta'$ S-wave contribution. Excluding now the $a_0(1450)$ (hypothesis 5) results in nearly the same χ^2 as for the best hypothesis (only slightly increased). The Dalitz plot corresponding to this hypothesis is shown in fig. 22.

The scan over different $a_0(1450)$ masses is reported in table 4. The other contributions are rather stable $\pm 0.2\%$. At the values used for the first fits the contribution is the highest. Mass values below 1400 MeV cause weak χ^2 dependence.

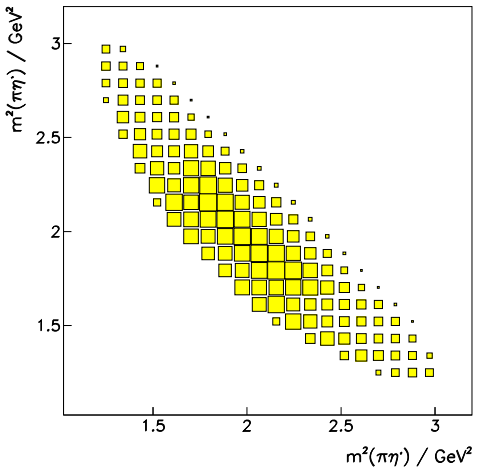

Figure 22:
The theoretical $\pi^0\pi^0\eta'$ Dalitz plot of hypothesis 5, exclude $a_0(1450)$ but introduce a $\pi^0\eta'$ P-wave.

m	Γ	χ^2	contribution / %
1490	280	130	4.8
1470	280	128	4.6
1450	280	126	4.3
1430	280	126	4.1
1410	280	126	4.0
1390	280	126	4.2
1450	270	128	4.2
1450	260	129	4.1
1430	270	127	4.0
1440	280	126	4.0

Table 4: Scan over different masses and widths for the $a_0(1450)$. The data set is not very decisive.

The same procedure is done for the $\pi^0\eta'$ P-wave and summarized in table 5. Also here the $\pi\pi$ S-wave and $a_2(1320)$ contribution practically does not change during the scan. The tendency is higher mass and larger width for the P-wave resonance.

After these exercises an optimum fit is achieved with an $a_0(1450)$ with a mass of about $m = 1430$ MeV and a width of $\Gamma = 280$ MeV and a P-wave resonance at about 1500 MeV having a width around 500 MeV. It is not decisive concerning the significance of $\pi^0\eta'$ S-wave against P-wave. We finally reach a $\chi^2 = 113$ (Neyman:

m	Γ	χ^2	contribution / %
1460	300	128	1.1
1440	300	129	1.2
1420	300	131	1.3
1405	300	132	1.4
1390	300	133	1.4
1380	300	134	1.5
1405	200	145	1.2
1405	250	137	1.3
1405	350	128	1.5
1405	350	128	1.5
1405	400	125	1.6
1405	500	122	1.7
1380	500	123	1.8
1520	500	116	1.4

Table 5: Scan over different masses and widths for the $\pi^0\eta'$ P-wave.

$\chi^2 = 121$; Pearson $\chi^2 = 113$). The contribution of both waves, $\pi^0\eta'$ S and P, is equal 0.6%. The $a_2(1320)$ intensity is $2.0 \pm 0.2\%$, where the error accounts already for the variation in all studies.

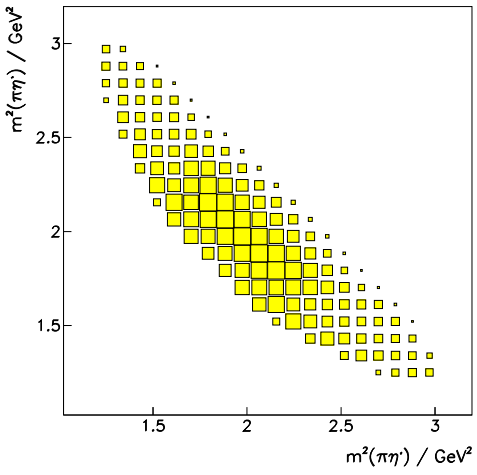

Figure 23:
The theoretical $\pi^0\pi^0\eta'$ Dalitz plot of , including $a_0(1450)$ and the $\pi^0\eta'$ P-wave according to hypothesis No. 6.

6 Conclusion

An amount of 3,559 $\pi^0\pi^0\eta'$ events have been prepared for the partial wave analysis. The final data set needs a $a_0(1450)$ or/and a exotic resonance at about 1500 MeV decaying into $\pi^0\eta'$ for a satisfactory description. The dominant contribution represents the $\pi^0\pi^0$I=0 S-wave as invented in previous analyses of 3 pseudoscalar final states.

From the coupled channel analysis [5] we get a product branching ratio for the $a_2(1320)$ $B(\bar{p}p\rightarrow\ a_2\pi^0; a_2\rightarrow\ \pi^0\eta) = 2.05 \pm 0.40)$. With the branching ratio eqn. 2 and the $\pi^0\eta'$ partial decay width as published by the VES collaboration [8] ($\Gamma_{\pi^0\eta'} = 106 \pm 32$ MeV) we calculate a a_2 intensity in $\pi^0\pi^0\eta'$ of $\alpha_{a_2} = (2.2 \pm 0.7)$ % , which compares well with the 2.0 ± 0.2 % found here.

The calculation cannot be done for the $a_0(1450)$, since it is the first observation of a $\pi^0\eta'$ decay of this resonance. With the $a_0(1450)$ branching ratio from the coupled channel analysis [5] of $(0.29\pm0.11)\cdot10^{-3}$ and a contribution of $a_0(1450)$ of (4 ± 0.3)% in case the P-wave resonance is not present, we get the ratio

$$R = \frac{B(a_0\rightarrow\ \pi^0\eta')}{B(a_0\rightarrow\ \pi^0\eta)} = 0.51 \pm 0.23 \tag{4}$$

A preliminary ratio was already determined in [9]: $R = 0.68 \pm 0.44$. On the other hand, allowing a P-wave contribution, we have seen that the $a_0(1450)$ intensity amounts only 0.6 ± 0.3% corresponding to $R = 0.08 \pm 0.05$.

The SU(3) flavour symmetry assuming coupling to the $(\bar{u}u + \bar{d}d)$ component of η and η' only, using the pseudoscalar mixing angle of $\Theta_{PS} = (-17.3 \pm 1.8)^o$ [10] predicts for the ratio R :

$$\begin{aligned} R &= \frac{q_{\pi^0\eta'}}{q_{\pi^0\eta}} \cdot \tan^2(90^\circ\ - \Theta_{id} + \Theta_{PS}) \\ &= 0.38 \pm 0.07 \end{aligned} \tag{5}$$

Here Θ_{id} is the ideal mixing angle 35.3^0 and $q_{\pi^0\eta'}, q_{\pi^0\eta}$ are the decay momenta of $a_0(1450)$. This value is in good agreement with the first number, or in other words, flavour SU(3) is fulfilled for $a_0(1450)$ if the P-wave is absent.

References

References

[1] E. Ferrer, private communication.

[2] C. Amsler et al., Phys. Lett. **B 333**(1994) 277 .

[3] C. Amsler et al., Phys. Lett. **B 297**(1992) 214.

[4] S.U. Chung et al., Ann. Phys. **4** (1995) 404.

[5] C. Amsler et al., Phys. Lett. **B 355**(1995) 425 .

[6] S. Baker and D. Cousins, Nucl. Instr. Meth. **221**(1984) 437.

[7] C. Amsler et al., Phys. Lett. **B 342**(1995) 433 .

[8] G.M. Beladize et al., Phys. Lett. **B 313**(1993) 276.

[9] S.Spanier, Dissertation, Mainz (1994).

[10] C. Amsler et al., Phys. Lett. **B 294**(1992) 415.